Neural Networks 179 (2024) 106502

Contents lists available at ScienceDirect

Neural Networks

journal homepage: www.elsevier.com/locate/neunet

Full Length Article

A computationally efficient and robust looming perception model based on dynamic neural field

Ziyan Qin[1], Qinbing Fu[1], Jigen Peng *

Machine Life and Intelligence Research Centre, School of Mathematics and Information Science, Guangzhou University, Guangzhou, 510006, China

ARTICLE INFO

Keywords:
Looming perception
Dynamic neural field
Adaptive lateral interaction
Dynamic threshold
Neural modeling
Robot dynamic vision

ABSTRACT

There are primarily two classes of bio-inspired looming perception visual systems. The first class employs hierarchical neural networks inspired by well-acknowledged anatomical pathways responsible for looming perception, and the second maps nonlinear relationships between physical stimulus attributes and neuronal activity. However, even with multi-layered structures, the former class is sometimes fragile in looming selectivity, *i.e.*, the ability to well discriminate between approaching and other categories of movements. While the latter class leaves qualms regarding how to encode visual movements to indicate physical attributes like angular velocity/size. Beyond those, we propose a novel looming perception model based on dynamic neural field (DNF). The DNF is a brain-inspired framework that incorporates both lateral excitation and inhibition within the field through instant feedback, it could be an easily-built model to fulfill the looming sensitivity observed in biological visual systems. To achieve our target of looming perception with computational efficiency, we introduce a single-field DNF with adaptive lateral interactions and dynamic activation threshold. The former mechanism creates antagonism to translating motion, and the latter suppresses excitation during receding. Accordingly, the proposed model exhibits the strongest response to moving objects signaling approaching over other types of external stimuli. The effectiveness of the proposed model is supported by relevant mathematical analysis and ablation study. The computational efficiency and robustness of the model are verified through systematic experiments including on-line collision-detection tasks in micro-mobile robots, at success rate of 93% compared with state-of-the-art methods. The results demonstrate its superiority over the model-based methods concerning looming perception.

1. Introduction

Looming perception, the ability of sensing approaching objects that signal imminent collision, is crucial for both living creatures and intelligent robots. The importance stems from considerations of safe interaction with environment or nearby objects as failing to perceive impending collisions can lead to serious consequences. To address this issue, numerous methods have been proposed to incorporate collision perception into intelligent systems, as reviewed in Franceschini (2014), Fu et al. (2019), Mukhtar et al. (2015). Over the last few decades, advanced sensors such as radar (Reich et al., 2020) and wireless ultraviolet communications (Zhao et al., 2022) have been employed in mobile robots, enhancing their navigation capabilities. Meanwhile, deep learning-based collision perception methods have been proposed, offering high accuracy and flexibility but are heavily reliant upon huge data from specific scenarios for training (Heiberg et al., 2022; Mukhtar et al., 2015). Besides, most of these aforementioned methods either require specialized sensors or involve extensive computation through map reconstruction, object detection, and estimation, and etc. Cigla et al. (2017), Gouda et al. (2013), Macias-Garcia et al. (2020), Mcfadyen and Mejias (2016), Schmidt and Wang (2014).

Nature can always provide us with abundant inspirations. Those looming perception methods based on research into biological visual neural systems exhibit a remarkable balance between computational efficiency and accuracy. Insects, for example locusts, despite their tiny brains, are capable of migrating in large groups over long distances without experiencing collisions. Studies have unveiled that within the visual system of locusts, the lobula giant movement detector (LGMD) neurons exhibit remarkable sensitivity to looming objects by showing the increasing and strongest response to looming stimuli, thus play a crucial role in triggering escape behaviors (O'shea et al., 1974; Rind, 1996). Driven by the biological research, certain models that leverage computing efficiency and energy consumption have been proposed (Fu

* Corresponding author.
E-mail addresses: ziyan9603@e.gzhu.edu.cn (Z. Qin), qifu@gzhu.edu.cn (Q. Fu), jgpeng@gzhu.edu.cn (J. Peng).
[1] Ziyan Qin and Qinbing Fu share first authorship.

https://doi.org/10.1016/j.neunet.2024.106502
Received 5 March 2024; Received in revised form 18 June 2024; Accepted 29 June 2024
Available online 3 July 2024

et al., 2019). These models perceive impending collision by the critical input generated from changes in the illumination of expanding object edges, rather than identifying or precisely locating specific moving objects (Chang et al., 2023; Fu et al., 2018; Lei et al., 2022; Rind & Bramwell, 1996; Yue & Rind, 2006).

Specifically, these models employ a hierarchical structure with several layers, normally the photoreceptor, excitation, inhibition, and summation layers, aiming to mimic characteristics of the acknowledged visual signal pathways pre-synaptic to the LGMD neuron in the optic lobe of locusts. The spatial–temporal competition between excitation and inhibition layers in summation layer, along with the critical input, contributes greatly to the looming selectivity of these bio-inspired models, showing heightened and strongest responses to looming stimuli. However, in the perspective of model response, this structure struggles to eliminate responses to receding stimuli and may also show false positives to other common visual movements such as translation. Such limitation likely leads to the generation of false collision alert especially for real-world scenarios. Besides, these models are computationally costly due to multi-layered signal filtering and processing.

Another approach to building looming perception framework originates from mathematical functions that elucidate non-linear relationships between angular size and angular velocity indicated by motion-induced inhibition and excitation, respectively (Gabbiani et al., 2002). For example, the well-established η-function assigns concrete link between such physical stimulus attributes and LGMD's activity, which is accessible to mathematical analysis (Hatsopoulos et al., 1995; Jones & Gabbiani, 2012). However, this leaves qualms about how to encode external moving stimulus to clearly indicate the angular velocity/size, and also lacks biological evidence on how such optical variables are neurally computed within the eyes.

Putting differently, dynamic neural field (DNF) is a brain-inspired neural framework that can be conceptualized as the average description of the activity dynamics of populations of neurons. The activation behavior of neurons within the field is dominantly determined by lateral interaction including lateral excitation and inhibition, and modulated by instant feedback signals within the field (Amari, 1977; Giese, 1999). In general, lateral excitation occurs among neurons in close proximity, while distal neurons typically provide lateral inhibition. Therefore, the lateral interaction kernel often represents a "Mexican hat" shape, that can be defined as a 'Difference of Gaussians' (DoG) kernel. The DoG kernel controls the scales of excitatory/inhibitory interaction respectively. By adjusting the interaction scales to maximize the excitatory signals caused by the expanding edges during looming course, while suppressing the excitation caused by the moving edge in other kinds of movements, the DNF framework has great potential of replicating the looming selectivity demonstrated by biological visual neural systems .

Hitherto, the DNF theory has a wide range of applications in the development of cognitive models, including those related to memory and learning (Jin et al., 2021; Qin et al., 2022b; Woodman et al., 2001). Its remarkable capability for processing continuous input sequences has also led to the utility of motion perception tasks for autonomous robots (Erlhagen & Schöner, 2002; Kamkar et al., 2022; Tan et al., 2016). Here we extended the DNF theory to align with the requirements of looming perception through introducing an adaptive lateral interaction mechanism for two specific reasons. Firstly, adaptation is one of the most important mechanisms in living organisms, and can be considered as an amazing approach to introduce adaptability into man-made systems. Adaptive interaction has also facilitated several neural networks to their performance (Brandt & Lin, 1999; Levina et al., 2009; McManus et al., 2011). Secondly, certain DoG-based techniques have been applied in photography to establish varying depths of field. In these techniques, the shape of DoG kernel plays a pivotal role in defining the extent of blur, which correlates with the distance between subject and observer (Pentland, 1987; Rafiee et al., 2013; Zhou et al., 2020). This can be related to the DoG kernel established in our looming perception model, which decides the areas of excitation and inhibition in lateral interaction. More specifically, a sharper DoG kernel implies a smaller blur area, which could indicate that the object is closer to the observer. In turn, the model responses can be enhanced for specific visual input by adaptively adjusting the DoG kernel-based interaction.

Additionally, to generate accurate responses across a range of orders of magnitude, we incorporated dynamic threshold to regulate spike generation to exert collision alert, and further shape the looming selectivity of our proposed model. Dynamic threshold is not only widely applicable in engineering, such as pattern recognition, edge detection and object detection (Hu et al., 2022; Liu et al., 2020; Liu & Yue, 2017) but also commonly observed in cortical and neural systems, as evidenced by numerous studies (Ding et al., 2022).

Combining adaptive interaction mechanism and dynamic threshold, the DNF-based looming perception model could be constructed as a single-field structure that stands out previous models with biological plausibility and straightforward formulation (model structure see Fig. 1). The intrinsic characteristic of DNF places a strong emphasis on inter-neuronal communication and instant feedback achieving the desired looming selectivity in an easily-built manner. Moreover, the two introduced mechanisms enhance the looming selectivity of the DNF model in complex and dynamic scenes. To validate the functionality of these mechanisms, we conducted ablation study accompanying mathematical analysis. We also carried out comparative experiments including off-line tests and on-line micro-robot tests in the real physical world to compare with a few state-of-the-art, model-based methods. The results unequivocally demonstrated the computational efficiency and robustness the proposed DNF model for looming perception across various scenarios. The main achievements of this research are abstracted as the following:

- This research exemplifies a simplified computational model built upon the DNF theory. The proposed DNF model selectively responds to looming stimuli while disregarding other typical motion patterns, such as receding, translating, elongation, and grating.
- Two pivotal mechanisms, namely adaptive lateral interaction and dynamic threshold, have been incorporated into the model to refine the looming selectivity. Notably, these two mechanisms have been relatively unexplored in both the insect visual system-based looming perception methods and the DNF literature. Additionally, we have conducted mathematical analysis to clarify the influence of adaptive lateral interaction on the iteration times needed to determine stationary solutions in DNF.
- With moderate adjustment, the proposed DNF model has been satisfactorily embodied in the embedded vision system of a micro-mobile robot, visually guiding the collision detection in autonomous navigation.

The rest of this paper is structured as follows: Section 2 reviews the literature. Section 3 presents the formulation with ablation study. Section 4 delves into the evaluation across real-world challenges. Section 5 introduces on-line micro-robot experiments. Further discussions are provided in Section 6. Section 7 concludes this paper. At last, the related mathematical analysis are furnished in Appendix A. All the abbreviations used in this paper and the variables of the proposed model are also listed in Appendix A.

2. Related work

This section briefly reviews relevant works in the areas of (1) bio-inspired models for looming perception, (2) DNF-based methods specializing in motion perception.

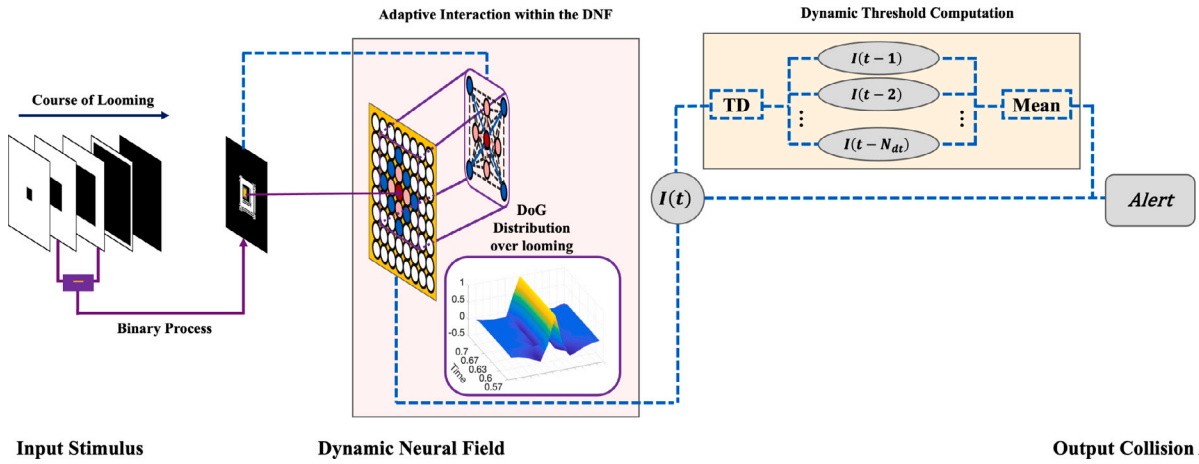

Fig. 1. The diagram of the proposed DNF-based looming perception model. The difference between successive frames in the input video is considered as the input images. Each neuron in the dynamic neural field corresponds directly to individual pixels within the images (for demonstration, the yellow pixel corresponds to the red neuron located in the DNF). Neurons within the field laterally interact with spatially adjacent neurons through excitation (depicted by the pink neurons in the diagram, representing neurons receiving excitatory lateral interaction) and inhibition (depicted by the blue neurons in the diagram, representing neurons receiving inhibitory lateral interaction). The lateral interaction in the model is governed by a DoG function, where the range of this interaction is controlled by the parameter σ in the DoG function. This range is adaptive and depends on the intensity of the input images. The DoG distribution throughout the looming process is illustrated in the inserted figure. The time axis in the figure represents the progression of time during the looming process. On the horizontal axis, the center cross-section of a three-dimensional DoG function is depicted, while the vertical axis indicates the values of the DoG function at each position along the center cross-section. The membrane potential of the neurons within the field is subsequently integrated as the neural field signal $I(t)$ using a sigmoid-like function. The neural field signals are temporally averaged using various time delays, labeled as "TD" in the figure. This averaging procedure draws inspiration from neuronal habituation, contributing to the establishment of a dynamic threshold, which in turn aids in generating final collision alerts within the model. It is noteworthy that all the solid purple lines in the diagram refer to pixel-wise computation, *i.e.*, each pixel or neuron has its own value, while all the blue dashed lines refer to computations or mechanisms when all the neurons within the field are integrated into a single signal.

2.1. Bio-inspired models for looming perception

Over millions of years of evolution, animals have developed remarkable ability of avoiding oncoming predators and imminent collisions despite their small bodies and tiny brains. Flies and locusts are renowned for looming perception and collision avoidance. A group of neurons known as lobula plate tangential cells (LPTCs) in flies play a critical role in the optic flow-based strategy (Borst, 2014; Serres & Ruffier, 2017). This strategy facilitates motion perception, a capability crucial for both unmanned and micro aerial vehicles (UAVs/MAVs) (Green & Oh, 2008; Meng & Yang, 2020; Milde et al., 2015; Park et al., 2019; Serres & Ruffier, 2017; Zhao et al., 2023). However, most of these methods are primarily designed for sensing lateral collision threats rather than frontal ones. Recently, researchers identified a neuropil called lobula plate/lobula column type-II cells (LPLC2) within the visual system of flies (Klapoetke et al., 2017). The LPLC2 neuronal ensemble exhibits the strongest response to dark objects approaching directly from the centroid of view, but not in the case of bypass or near-miss. This discovery has also inspired researchers to proposing new collision detection methods (Hua et al., 2022; Zhao et al., 2023b; Zhou et al., 2022).

The locust's LGMD, on the other hand, respond to wide-field motion regardless the direction, and exhibits the highest firing rate on looming object among other visual stimuli (Olson et al., 2021; Rind & Bramwell, 1996; Wang et al., 2018; Zhu et al., 2018). Drawing inspiration from presynaptic neural circuits of LGMD, a range of looming perception methods have been gradually developed. These methods offer advantages of computing efficiency, and flexibility for ground vehicles, UAVs, and other vision-based robots (Fu et al., 2020a; Salt et al., 2017; Yue et al., 2006; Zhao et al., 2019). Notably, taking into account the biologically plausible ON/OFF pathways and spike frequency adaptation mechanism in the locust's visual system, Fu et al. further developed two collision perception visual systems that replicate the specific looming selectivity of two LGMD neurons, namely, LGMD1 (Fu et al., 2018) and LGMD2 (Fu et al., 2020a). In particular, the LGMD2 model incorporates temporal adaptive lateral inhibition to realize the specific responsive characteristics of genuine LGMD2 circuit. Another LGMD-based neural model is proposed by Lei et al. (2022), presenting a model that eliminates the model response to translating by ON/OFF neural competition. One of the most recent studies explores the feedback loop through parallel ON/OFF channels in an LGMD-based neural network (Chang et al., 2023). This model propagates output signals from ON/OFF channels back to their respective starting neurons, aiming to backtracking extracted motion information to the lower-level neurons to achieve different looming selectivity to ON/OFF contrast.

Typically, the LGMD-based neural network models discussed above follow similarly a multi-layered, hierarchical structure with various additional mechanisms. While these models exhibit strongest response to looming stimuli, their responses to other motion stimuli, such as receding and translating, can sometimes be challenging to differentiate from looming stimuli based on their spiking output. This limitation usually results in false positives when integrated into autonomous robots (Fu et al., 2019).

Gabbiani and his colleagues also established a mathematical expression called the η–function to illustrate the relationship between the physical attributes of visual stimulus and the firing rate of LGMD model (Hatsopoulos et al., 1995). The η–function is a multiplicative combination of object's angular size and angular speed, through a logarithmic–exponential transform. By comprehensive experiments and mathematical analysis, the authors claimed that the peak time relative to the collision is relative to the ratio of $l/|v|$, where l is the half size of approaching object and $|v|$ is the constant approaching speed of the object. This linearity remains regardless of body temperature, background luminance, target shape, target texture and target approaching direction (Fotowat & Gabbiani, 2011; Gabbiani et al., 1999, 2001). In general, the whole η–function theory is based on the ratio $l/|v|$, and the angular size and angular velocity of the looming object that projected on the retina. However, the ratio $l/|v|$ is impossible to obtain and varying each frame in real-world scenarios, besides, the encoders of angular size and angular velocity in the visual systems of locusts are unexplored.

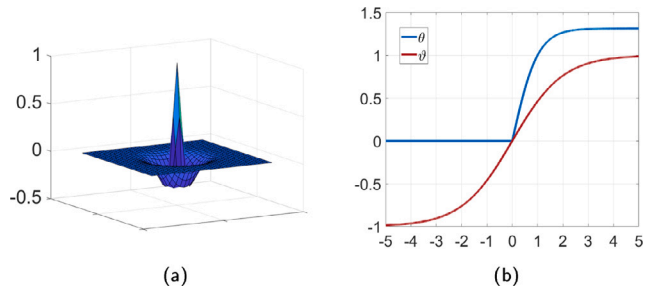

Fig. 2. The lateral interaction kernel,threshold function ϑ and the activation function θ of the proposed model. (a) The DoG kernel exhibits a 'Mexican hat' shape and serves to regulate lateral interactions within the field. (b) The threshold function ϑ for lateral interaction is depicted in red, it is symmetrical as neurons receive both excitatory and inhibitory interactions. The activation function θ for the neurons in the field, depicted in blue, is a hyperbolic tangent (tanh) function normalized by $\tanh(1)$.

2.2. DNF-based methods specializing in motion perception

DNF is a mesoscopic model that describes the average activation of a group of similar neuron with the formulation of ordinary differential equations (ODE) (Amari, 1977; Kwessi, 2021; Quinton & Goffart, 2018). By setting different functional layers, researchers have already implemented this framework into cognitive robots, facilitating their performance on path planning, obstacle avoidance (Erlhagen & Schöner, 2002; Tan et al., 2016). However, the DNF model has been scarcely applied to looming perception. This may be due to the inability to distinguish between different stimuli when using a fixed lateral interaction scale or the high computational requirements for solving the stationary solution of ODE (Qin et al., 2022a). In conjunction with computer vision techniques, a recent study has implemented a DNF-based model for multi-target tracking with a computational cost of just 0.19 s per frame (Kamkar et al., 2022). While this work offers promise for DNF-embedded micro-robotics, there remains a necessity to propose new mechanisms aimed at further reducing the computational burden of the DNF-based methods.

In this regard, we introduced the adaptive lateral interactions, which utilize the input itself to dynamically adjust the lateral interaction scale. This mechanism enhances the ability to distinguish between different types of moving stimuli in the DNF-based model. Additionally, we incorporated a dynamic threshold-based spike mechanism to improve the model's selectivity to merely looming stimuli. After making adjustments to propagation delays, a technique similar to the approach discussed in the DNF literature (Burlakov et al., 2021; Solak et al., 2023; Spek et al., 2020), we satisfactorily integrated this model into embedded vision of a micro-robot for collision detection in autonomous navigation.

3. Formulation and corroboration

In this section, we present the formulation of the proposed model, and the ablation study on the introduced mechanisms, that is, the adaptive lateral interaction and the dynamic activation threshold. The proposed model is built upon a single-field DNF, which takes visual streams as input for both off-line and on-line experiments. Notably, the input also regulates the lateral interaction scale of the model with respect to time. After resolving the stationary solution of the ODE in DNF, the activation of each neurons within the field are integrated with even weightings, and subsequently employed to generate spike depending on dynamic threshold, leading the production of collision alert indicated by successive spikes.

3.1. The proposed DNF model

There are various forms of DNF, and for the formulation of the proposed looming perception model, we utilize the typical Amari's DNF theory from Amari (1977). As illustrated in Fig. 1, the inputs for the proposed model are visual streams from captured images with the resolution of $m \times n$. It is assumed that each pixel in the video or image corresponds directly to a neuron in the field of vision. Therefore, the perceptive field Ω of the DNF consists of $m \times n$ neurons. The membrane potential of a neuron, denoted as $u(x, y, t)$, corresponds to a pixel in the input video located at spatial coordinates (x, y) and at time t. To be specific, as we only consider the stationary solution for the computation, the time t specifically refers to the time in input stimuli. Then $u(x, y, t)$ can be regulated as follows:

$$\frac{\partial u(x,y,t)}{\partial t} = -\frac{1}{\tau}u(x,y,t) + S(x,y,t) - h + \vartheta\Big(\iint_{\Omega} w(x-i, y-j, t)u(i,j,t)\,dx\,dy\Big) \tag{1}$$

The parameter τ represents the time scale of neural activation. Given that this is a single-field DNF model, we set $\tau = 1$ for simplicity. The external input $S(x, y, t)$ for the neurons is a binary value that is determined by the absolute change in luminance between every two successive frames, which is

$$S(x,y,t) = \begin{cases} 1, & \text{if } |L(x,y,t) - L(x,y,t-1)| > 0, \\ 0, & \text{otherwise.} \end{cases} \tag{2}$$

$L(x, y, t)$ and $L(x, y, t-1)$ are the gray-scaled brightness of two successive frames, and the gray-scaled value range of all the input stimuli in this paper is within the range of $[0, 1]$. This binary transformation indeed reduces significantly the effect by contrast between foreground looming object and background optic flow. The reversal potential is denoted by h and is empirically set as a constant value of 0.2. The last term of the right side of the equation describes the lateral interaction that this neuron receives in the field. As lateral interaction can be either positive or negative, the threshold function ϑ is symmetrical about the origin and is defined as (see Fig. 2(b), red curve):

$$\vartheta(u) = \frac{2}{1+e^{-u}} - 1$$

The lateral interaction kernel, denoted as $w(x - i, y - j, t)$, in the DNF typically exhibits a "Mexican hat" shape (see Fig. 2(a)). This implies that the inhibitory interaction scale of a neuron is larger than the excitatory interaction scale. In this paper, we use Difference of Gaussians (DoG) kernel as the lateral interaction kernel:

$$w(x-i, y-j, t) = A\exp\Big(-\frac{(x-i)^2 + (y-i)^2}{2\sigma_1(t)^2}\Big) - B\exp\Big(-\frac{(x-j)^2 + (y-j)^2}{2\sigma_2(t)^2}\Big) \tag{3}$$

where the $\sigma_1(t)$ and $\sigma_2(t)$ represent the excitatory interaction scale and the inhibitory interaction scale of a neuron with respect to time, respectively. Similarly with some DNF study, we set the relationship between the two scales as $\sigma_2(t) = 3\sigma_1(t)$ (Jin et al., 2021; Qin et al., 2022b). Consequently, we obtain the values $A = 3/2$ and $B = 1/2$. Due to the substantial difference between the inhibitory and excitatory lateral interaction scales, and the fact that the activation behavior of neurons within the field falls within a similar range, the majority of neurons within the field receive inhibitory lateral interactions. The exception to this general pattern is found among neurons corresponding to the pixels located at the edges of moving stimuli.

Importantly, without changing the basic shape of lateral interaction kernel, the adaptive lateral interaction is achieved by adjusting the excitatory scale $\sigma_1(t)$ according to the input intensity. The adaptation can be mathematically described as:

$$\sigma_1(t) = \sigma_0 - \frac{\iint_{\Omega} |L(x,y,t) - L(x,y,t-1)|\,dx\,dy}{\iint_{\Omega} S(x,y,t)\,dx\,dy} \tag{4}$$

The initial excitatory lateral interaction scale is settled as $\sigma_0 = 1$. The input intensity is calculated as the average luminance change per changed pixel. The standard deviation gradually increases for looming

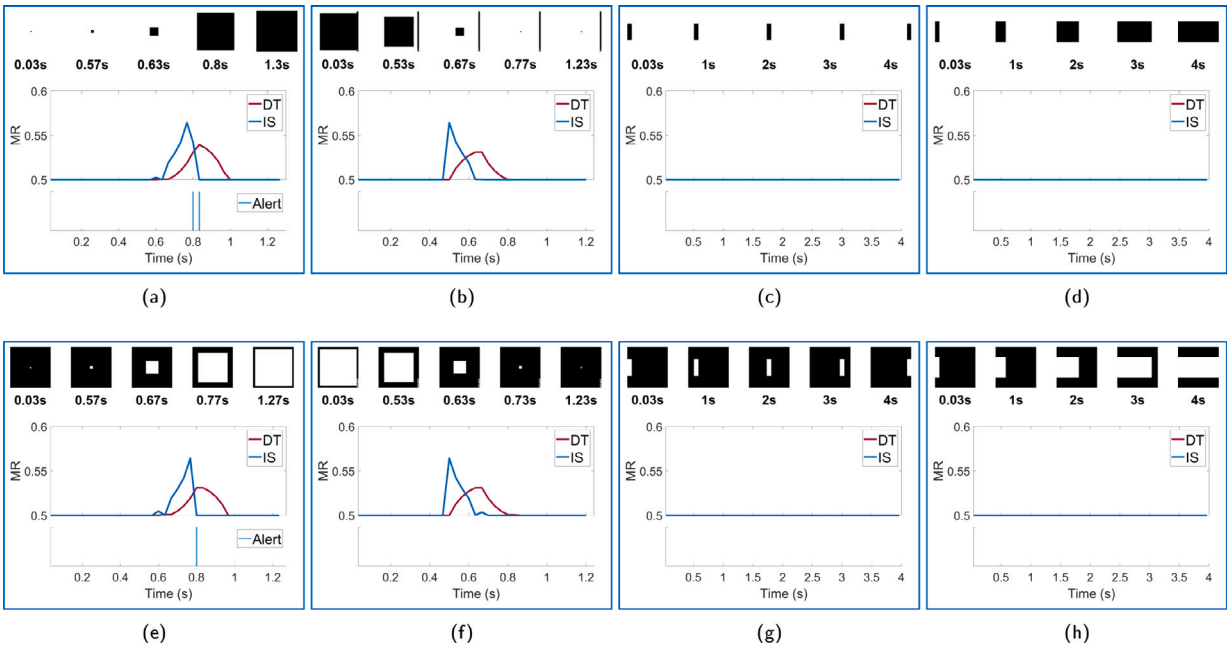

Fig. 3. The model responses of the proposed model to 10 synthetic stimuli are shown in the figure. Each sub-figure displays the snapshot of the tested synthetic stimuli in the first row, the model responses (abbreviated as IS in the figure) and the dynamic threshold (abbreviated as DT in the figure) in the second row, and the occurrence of collision alert in the last row.

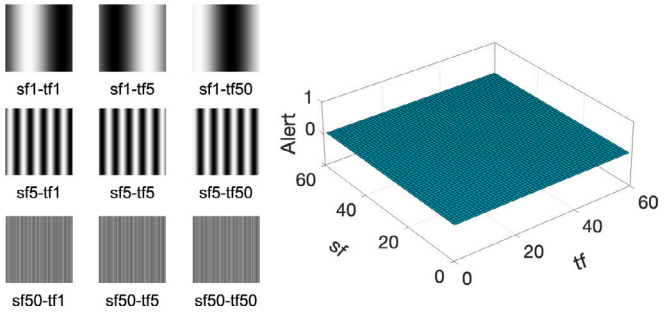

Fig. 4. The proposed model does not respond to grating stimuli under different spatial/temporal frequencies. Examples of the testing grating stimuli are shown on the left, with the snapshot at 1 s. Higher temporal frequency (abbreviated as tf in the figure) indicates faster movement of the stripes, while higher spatial frequency (abbreviated as sf in the figure) indicates thinner stripes in the grating stimuli. The model's responses to the testing stimuli are shown on the right, where 0 represents that the model does not generate a collision alert, vice versa for 1.

objects, decreases for receding objects, and remains relatively stable for translational motions, such as translating, elongation, and grating stimulus. Therefore, the excitatory interaction scale, $\sigma_1(t)$, gradually decreases for looming stimuli but increases for receding stimuli. Smaller lateral interaction scales for the neurons have a minimal negative impact on the membrane potential of neurons, and in some cases, they even increase it. This is because smaller lateral interaction scales barely decrease the membrane potential of neurons, while also reducing inhibitory lateral interactions, which can potentially increase the membrane potential of other neurons. In contrast, larger lateral interaction scales indicate not only larger excitatory lateral interactions but also inhibitory lateral interactions three times greater in magnitude. As a result, these larger scales tend to decrease the membrane potential of the neurons within the field more than they increase it. This asymmetry in the lateral interaction scale is a key characteristic of the model, making it more responsive to specific looming stimuli while suppressing responses to others.

The membrane potential of each neuron undergoes an activation function before being integrated. We select the activation function in the shape of a hyperbolic tangent (tanh) function, based on the research of neuron firing rates (Dayan & Abbott, 2002). However, we normalize it by tanh(1) to further amplify the membrane potential to benefit the model performance on real-world scenarios. The activation function, as shown in Fig. 2(b) and represented by the blue curve, is expressed as:

$$\theta(u) = \frac{e^u - e^{-u}}{e^u + e^{-u}} \cdot \frac{e^2 + 1}{e^2 - 1}.$$

Subsequently, the firing rates of all the neurons in the field can be evenly-weighted integrated and non-linearly activated by a sigmoid function:

$$I_u(t) = \frac{1}{1 + exp(-\iint_\Omega \theta(u(x, y, t))\, dx\, dy \cdot (mn)^{-1})}. \tag{5}$$

To ensure precise responses across a wide range of magnitudes, we introduce the mechanism of dynamic threshold to regulate the spike generation. For the sake of simplicity in engineering applications, the dynamic threshold is often expressed as a percentage of the maximum value (Liu & Yue, 2017) or the value of a specific sample within a data sequence (Shi et al., 2021). In this paper, we establish the dynamic threshold by simulating a basic neuronal characteristic, habituation. To be specific, neurons would become harder to activate if their previous membrane potentials have been consistently increasing. The threshold is settled temporally as the average of previous signals in a short time window N_{dt}:

$$I_{thre}(t) = \frac{\int_p^{t-1} I_u(t)dt}{N_{dt}}, \tag{6}$$

where N_{dt} is set as 5 in this paper and $p = t - N_{dt} - 1$. Typically, the integrated signal of the proposed model would gradually increase as the looming object gets closer, activating more neurons within the neural field. Therefore, a smaller value for N_{dt} makes the neuron harder to overstep the spike threshold in this scenario.

A spike is generated if the integrated signal surpasses the dynamic threshold, as expressed in the following equation:

$$\text{spike(t)} = \begin{cases} 1, & \text{if } I_u(t) > I_{thre}(t), \\ 0, & \text{otherwise.} \end{cases} \tag{7}$$

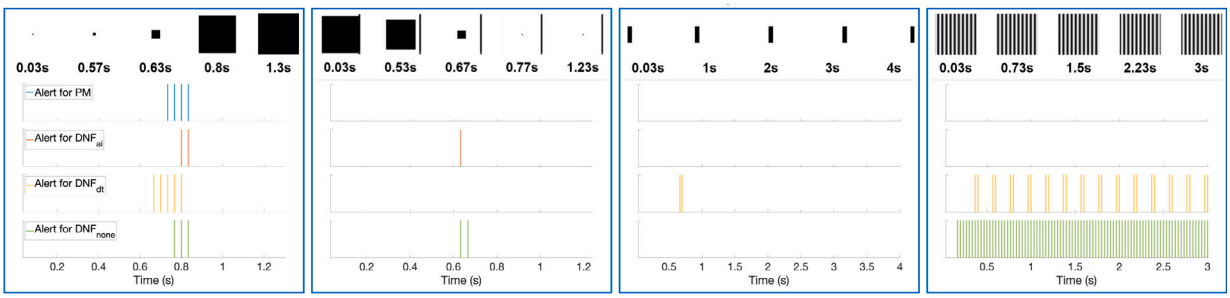

Fig. 5. The response of the proposed model (abbreviated as PM), the DNF model with adaptive lateral interaction (abbreviated as DNF_{ai}), the DNF model with dynamic threshold (abbreviated as DNF_{dt}), and the original DNF model without adaptive lateral interaction and dynamic threshold (abbreviated as DNF_{none}) against the 4 sets of synthetic stimuli is shown. The first row of each sub-figure displays the snapshot of the test stimuli, and the subsequent rows show instances of collision alerts generated by these models, respectively. Notably, in sub-figure (c), the integrated signals $I_u(t)$ of DNF_{dt} and DNF_{none} are always below the fixed threshold 0.52 but above the dynamic threshold in DNF_{dt} since the dynamic threshold is strongly related to $I_u(t)$. Thus, collision alerts would be generated at the beginning of the moving stimuli in DNF_{dt} but always eliminated in DNF_{none}.

To avoid false alarms, only a number of successive spikes can trigger the collision alert. This can be defined as:

$$\text{Alert(t)} = \begin{cases} 1, & \text{if } \sum_{n=q}^{t} \text{spike}(n) = N_{spk}, \\ 0, & \text{otherwise.} \end{cases} \tag{8}$$

where $N_{spk} = 4$ represents the number of spikes within a specific time that are required to trigger an alert, and this specific time interval starts at $q = t+1-N_{spk}$. This value is consistent with the previous LGMD-based models. The computation process of the proposed looming perception model is summarized as algorithm 1, the fixed point iteration process and dynamic threshold involved spike mechanism are also included in this algorithm.

Through the formulation above, we can observe that the scale of parameters of the proposed single-field DNF model is quite small that brings benefit of adjusting the model to different looming scenarios. Accordingly, the proposed model is tractable and the learning methods are currently not involved in the framework.

Algorithm 1: Looming perception based on DNF

input : $L(x, y, t)$, σ_0, h, N_{dt}, N_{spk}
output: Alert(t)

for $t = 2 : T$ **do**
- Obtain the input video frames $L(x, y, t)$ and $L(x, y, t-1)$;
- Compute the input of the DNF via Eq. (2);
- Compute the σ_1 and σ_2 in DoG kernel via Eq. (4);
- Compute the DoG kernel via Eq. (3);
- `// fixed-point iteration process`
- Initial $u(x, y, t, t_f) = -h$, where $x \in [1, m]$ and $y \in [1, n]$. Set fix point iteration times $t_f = 0$;
- Compute $u(x, y, t, t_f)$ through the stationary solution equation: $u(x, y, t, t_f) = S(x, y, t) - h + \vartheta\big(\iint_\Omega w(x-i, y-j, t)u(i, j, t, t_f - 1)\,dx\,dy\big)$ and set $t_f = 1$;
- Compute the $error = u(x, y, t, t_f) - u(x, y, t, t_f - 1)$;
- **while** $error > 0.01$ **do**
  - Compute $u(x, y, t, t_f)$ through the above stationary solution equation;
  - Set $t_f = t_f + 1$;
  - **if** $t_f > 10$ **then**
    - break
- `// end while`
- Use the final $u(x, y, t, t_f)$ to generate integrated signal via Eq. (5);

`// Dynamic threshold involved spike mechanism`
for $t = N_{dt} : T$ **do**
- Generate the threshold via Eq. (6);
- Compare the integrated signal and threshold via Eq. (7);

`// Collision alert`
for $t = N_{spk} : T$ **do**
- Final collision alert generation $Alert(t)$ via Eq. (8);

3.2. Ablation study

The proposed model was initially evaluated using simple synthetic stimuli that share the resolution of 100 × 100, at 30 frames per second. The response of the proposed model against synthetic stimuli can be seen in Fig. 3. Some stimuli depict a dark or white square either approaching or receding against a white or dark background (see (a),(b),(e) and (f) in Fig. 3), and other stimuli portray a dark or white bar translating or elongating from the left to the right (see (c),(d),(g) and (h) in Fig. 3). We also tested grating patterns with different spatial and temporal frequencies respectively (see Fig. 4). Both Fig. 3 and Fig. 4 illustrate the model's response, showing that it responds selectively to looming stimuli while remains inactive for other types of motion stimuli.

We proceeded ablation studies to elucidate the effects of the two proposed mechanisms on shaping the looming selectivity. Since we calculate the input for the model as the binary value of the differential images of successive gray-scale frames, the input would be identical when processing synthetic stimuli that depict the same object motion but with converse contrast between moving object and its background, such as dark object approaching and light object approaching. Similarly, the input would be similar for stimuli representing translation and elongation, as the model perceives both of these stimuli as a bar moving from side to side. For illustrative purposes, we thus conducted ablation studies using the following input stimuli: dark square approaching and receding, dark bar translating, and a grating pattern.

We evaluated the model performance of the proposed model, the DNF model with adaptive lateral interaction, and the DNF model with dynamic threshold using the same synthetic stimuli. In addition, the original DNF model without adaptive lateral interaction and dynamic threshold is also taken into comparison. For the DNF model with adaptive lateral interaction and the original DNF model, the threshold for spike generation is empirically set to $I_{thre} = 0.52$. Meanwhile, in the DNF model with dynamic threshold and the original DNF model, the excitatory interaction scale is established as $\sigma_1 = 0.2$ to provide optimal performance for looming perception, as previously determined (Qin et al., 2022a). The remaining settings of these two investigated models are consistent.

Table 1
Responses of various models to basic synthetic stimuli.

Stimuli	Proposed model	LGMD1 2022ver.	LGMD1	LGMD2	F-LGMD ONn	F-LGMD ONp
Dark Approaching	1 (✔)	1 (✔)	1 (✔)	1 (✔)	1 (✔)	1 (✔)
Light Approaching	1 (✔)	1 (✔)	0 (✖)	0 (✖)	0 (✖)	1 (✔)
Dark Receding	0 (✔)	1 (✖)	1 (✖)	0 (✔)	0 (✔)	1 (✖)
Light Receding	0 (✔)	1 (✖)	1 (✖)	0 (✔)	1 (✖)	1 (✖)
Dark elongation	0 (✔)	1 (✖)	1 (✖)	0 (✔)	0 (✔)	0 (✔)
Light elongation	0 (✔)	1 (✖)	0 (✔)	0 (✔)	0 (✔)	0 (✔)
Dark translating	0 (✔)	0 (✔)	1 (✖)	0 (✔)	0 (✔)	0 (✔)
Light translating	0 (✔)	0 (✔)	1 (✖)	0 (✔)	0 (✔)	0 (✔)
Grating1	0 (✔)	0 (✔)	0 (✔)	0 (✔)	1 (✖)	1 (✖)
Grating2	0 (✔)	0 (✔)	0 (✔)	0 (✔)	1 (✖)	1 (✖)

1 1 represents that the model generates collision alerts for the corresponding stimulus, while 0 signifies non-response;
2 (✔) behind the number represents true positive or true negative, while (✖) represents false positive or false negative;
3 The selectivities of these comparative models might differ from those reported in their original papers due to variations in parameter settings.

Fig. 5 illustrates the results of ablation study. It can be abstracted that the use of dynamic threshold eliminates the model's responses to receding stimuli. This happens because the integrated signal is stronger at the beginning of receding, which in turn leads to a higher dynamic threshold for generating a spike and subsequently suppresses the model's response. Such dynamic threshold almost stays the same for translating or grating stimulus since these two motion patterns induce relatively stable integrated outputs.

On the other hand, the adaptive lateral interactions eliminate the model's response to translating and grating stimuli because those motion patterns exhibit relatively stable and weaker input intensities, which keep the scale of lateral interaction, *i.e.*, inhibitory interaction scale steadily larger compared to approaching stimulus and thus suppress the model's response. For stimuli like receding, the gradually decreasing input intensity leads to an increase in the lateral interaction scale. However, the model without the dynamic threshold still generates an alert based on its response at the beginning of receding, even though the model's response is immediately suppressed. Taking together, the basic looming selectivity is accomplished by the single-field DNF model, and further enhanced by the proposed two mechanisms.

4. Comparative experiments

Within this section, we demonstrate advantages of the proposed single-field DNF model regarding computational efficiency and robustness of addressing real-world, complex visual tasks. We compared the proposed model with five state-of-the-art looming perception models, including the LGMD1-based model proposed by Fu et al. (2018) (abbreviated as LGMD1), the LGMD2-based model proposed by Fu et al. (2020a) (abbreviated as LGMD2) that features specific selectivity to only darker looming objects, the LGMD1-based model that eliminates the response to translating motion proposed by Lei et al. (2022) (abbreviated as LGMD1 2022ver.), and the LGMD model with feedback proposed by Chang et al. Specifically, in the LGMD-based model with feedback, we constructed both positive feedback circulating the ON pathway (abbreviated as F-LGMD ONp) and negative feedback (abbreviated as F-LGMD ONn) for comparison. The reason behind is this feedback model represents diverse selectivity, with which the F-LGMD ONn shows looming selectivity to only OFF-contrast stimulus as exhibited by the LGMD2 neurons while the F-LGMD ONp demonstrates looming selectivity comparable to the LGMD1 neuron (Chang et al., 2023).

For all off-line experiments undertaken in this paper (including the ablation studies in Section 3.2), the implementation of all investigated and compared models, the data analysis and visualization were accomplished in Matlab (The MathWorks, Inc., Natick, USA), conducted on a computer with an Intel Core(TM) i5-10500 CPU processor and 16 GB of RAM. All the video sequences used for real-world scenarios testing are collected and detailed in the *Supplementary Materials*. To enhance the DNF model response to real-world scenarios, we lower the initial value of lateral interaction scale σ_0 from 1 to 0.618. The configuration of other parameters remains the same as the ablation study.

4.1. Criterion for model comparison

To quantify the effectiveness of looming perception for all the investigated and compared models, we adopted a standard criterion indicating the accuracy of perception as the ratio of all tested data for which the model produces correct responses using the following formula:

$$accuracy = \frac{TP + TN}{TP + TN + FP + FN} \times 100\% \tag{9}$$

Precisely, TP is short for "true positives" indicating the number of tested stimulus for which the model generates correct collision alerts for genuine collision scenarios. This is calculated by the model releasing its initial alert to approaching objects at or before the instant of collision. FP is short for "false positives" denoting the number of tested data for which the model erroneously generates collision alerts to non-colliding stimuli, such as translational, near-miss, or receding stimulus. TN, *i.e.*, "true negatives", represents the number of tested stimulus for which the model is not responding to non-colliding stimulus. Lastly, FN stands for "false negatives" accounting for the number of tested data for which the model fails to detect collision.

4.2. Results with analysis

Firstly, in order to showcase the basic looming selectivity of the comparative models, we conducted experiments using the synthetic stimuli identical to the ablation studies in Section 3.2. The results are elaborated on Table 1. It can be seen from the table that all of the investigated models including the proposed DNF model respond to looming motion well, and only the LGMD1 model respond to non-looming, *i.e.*, the translating stimuli. Notably, only the proposed DNF model and the LGMD2 model are resistant to receding stimuli. Although the LGMD1 2022ver. model represents non-response to translating, it is yet affected by dark/light elongation of a single edge translating. In general, the LGMD2 model and the proposed DNF model outperform the other comparative models in synthetic stimuli tests. The LGMD2 model nevertheless is non-sensitive to light approaching, *i.e.*, ON-contrast stimulus owing to its specific selectivity to OFF-contrast.

Secondly, we employed a variety of real-world scenes to compare the aforementioned neural models. This category of data includes structured indoor scenes like balls looming, receding, and translating in front of a white background, as well as unstructured, dynamic outdoor scenes such as car driving, UAV flight scenarios. These videos were collected at different resolutions and frame rates. The details of testing data can be found in the *Supplementary Materials*.

Fig. 6 represents the corresponding results of all investigated and compared models challenged by the real-world stimuli. Fig. 7(a) along with Table 2 statistically show the accuracy of all investigated and compared models in this case. In addition, the computational efficiency

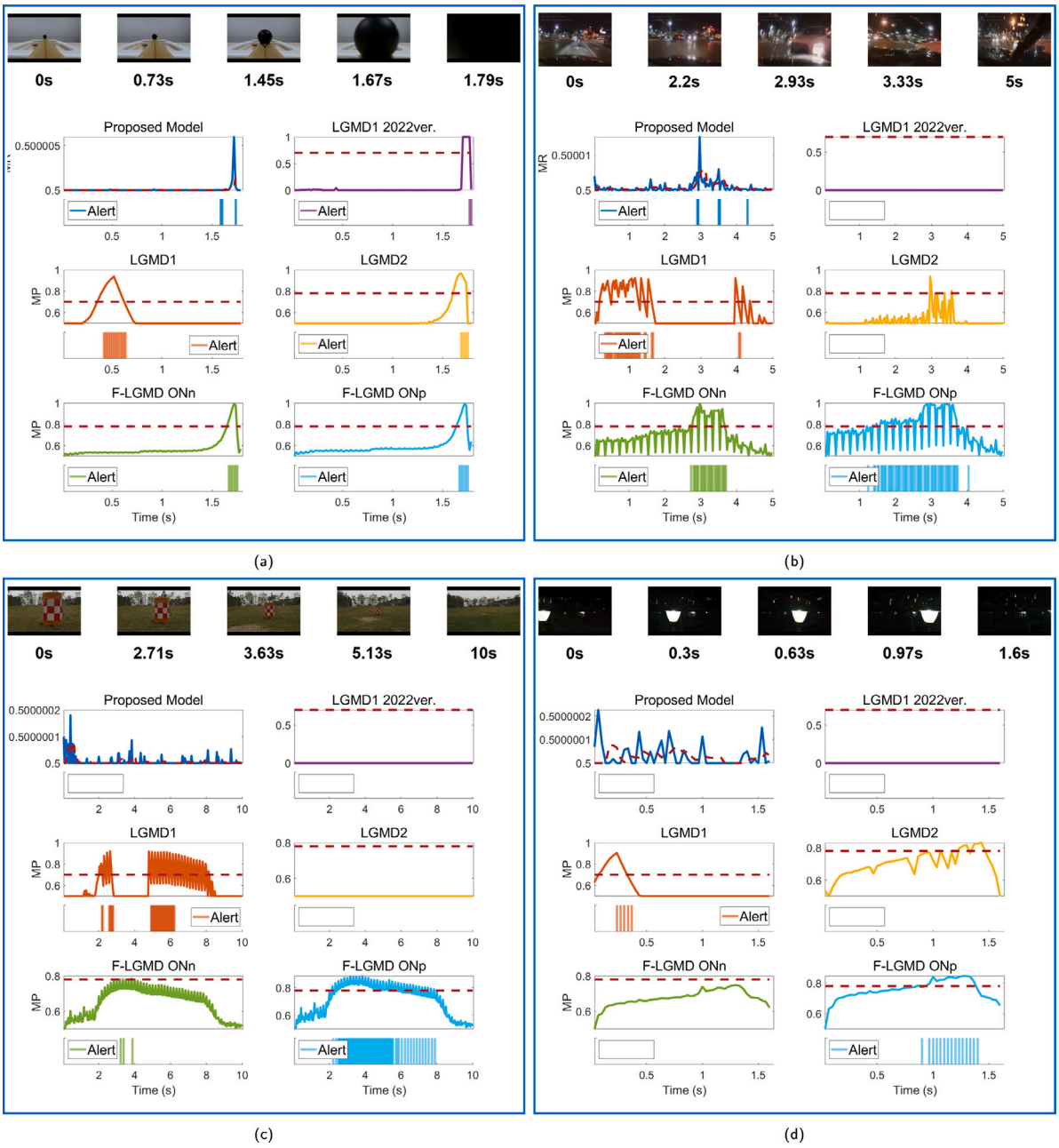

Fig. 6. The model response for the proposed model and the comparative LGMD-based models. For each sub-figures, the first display the snapshots of the preceding stimulus, the model output (the integrated signal for the proposed model and the membrane potential for the comparative models) and their threshold are plotted below, along with the occurrence of collision alerts. The experiments cover various scenarios: (a) dark ball approaching, (b) car approaching then crashed at night, (c) UAV receding from a barrier, and (d) UAV translating relative to a night road lamp.

Table 2
Accuracy (%) of various models to 47 real-world data sets in total.

Stimuli	Proposed model	LGMD1 2022ver.	LGMD1	LGMD2	F-LGMD ONn	F-LGMD ONp
Ball	**100%**	58.33%	0%	**100%**	**100%**	**100%**
UAV	**85%**	65%	10%	65%	30%	10%
Car Crash	**53.33%**	26.67%	13.33%	26.67%	**53.33%**	20%
Overall	**78.72%**	51.06%	8.51%	61.7%	55.31%	36.17%

measured by average computing time per frame of all the investigated and compared models is illustrated in Fig. 7(b), and numerically elaborated on Table 3. More specifically, the proposed DNF model generates collision alerts for dark ball approaching and car crash, while remaining silent for visual movements including barrier receding and road lamp translating recorded through the view of UAV during flight. Likewise, the LGMD1 2022ver. model and LGMD2 model are silent to barrier receding and road lamp translating, nevertheless, activated by car approaching as shown in the sub-figure (b) in Fig. 6. The LGMD1 model generates collision alerts for ball approaching at the beginning of looming process, which can be considered as a false alert at the early stage of looming process. Besides, the LGMD1 model also

Table 3
Average computational time per frame (seconds) of various models to 47 real-world data sets.

Stimuli	Proposed model	LGMD1 2022ver.	LGMD1	LGMD2	F-LGMD ONn	F-LGMD ONp
Ball	0.06	**0.011**	0.056	0.06	0.035	0.034
UAV	0.059	**0.012**	0.056	0.06	0.036	0.034
Car Crash	0.016	**0.003**	0.017	0.017	0.006	0.006
Overall	0.045	**0.009**	0.043	0.047	0.026	0.025

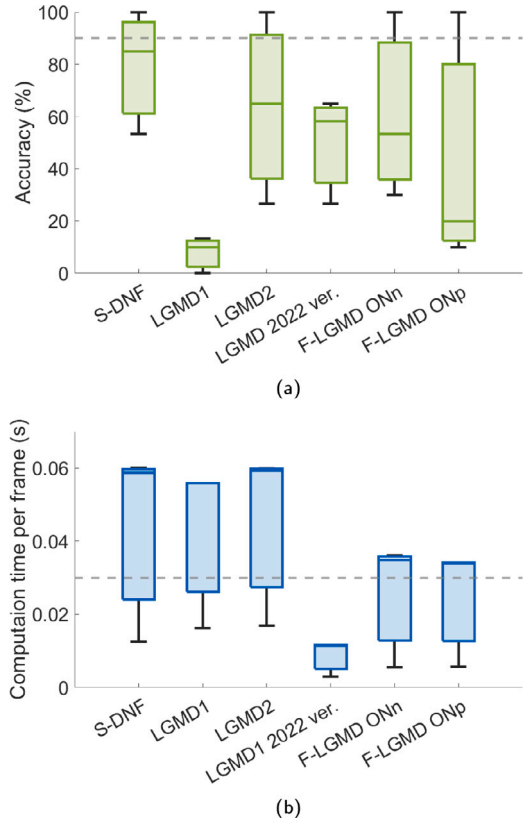

Fig. 7. Box plots that are constructed based on experiment results from the proposed model and the 5 comparative models on the real-world data sets: (a) the collision detection accuracy; (b) the computational time per frame.

erroneously generates collision alerts for the other stimuli shown in Fig. 6. Similar to the LGMD1 model, the F-LGMD ONn and F-LGMD ONp models respond to car crash too early and incorrectly respond to barrier receding, despite generating collision alerts for the dark ball approaching stimulus, timely. In the perspective of looming perception accuracy calculated by Eq. (9), the proposed DNF model exhibits the highest accuracy thus outperforms all the comparative, state-of-the-art models.

Regarding the computational efficiency, the proposed model is comparable to the LGMD1 and LGMD2 models. As the previous studies have shown the computational simplicity and efficiency of the LGMD1 and LGMD2 models on board micro-mobile robot for real-time visual processing (Fu et al., 2019), the proposed DNF model has potential to be implemented as embedded vision system as the similar computing time measured in this research. The LGMD1-2022ver. model, albeit achieves the shortest computational time, reaches the accuracy around only 50% of all tested data. In contrast, the F-LGMD ONn model demonstrates better accuracy compared to the LGMD1 2022ver. model but comes at the cost of nearly three times the computational time. The F-LGMD ONp, on the other hand, exhibits a similar computational time to F-LGMD ONn but with lower accuracy. It is worth emphasizing here all the comparative models are biologically inspired, model-based approaches. The data-driven methods like deep-learning models are not requisite for comparison in this paper.

5. Verification of robotic embedded vision

We continued our experiments to program the proposed DNF model into the embedded vision system on board a micro-mobile robot named *Colias*, which has been used for research into bio-inspired motion perception visual systems (Fu et al., 2019). As analyzed in the off-line experiments, the proposed DNF model demonstrates comparable computing efficiency to the related bio-inspired models for robot vision. To accelerate the proposed DNF model, we introduced the propagation delay to replace the solution of fixed point iteration as

$$\frac{\partial u(x,y,t)}{\partial t} = -\frac{1}{\tau}u(x,y,t) + S(x,y,t) - h + \vartheta\Big(\sum_{i=1}^{m}\sum_{j=1}^{n} w(x-i,y-j,t)(u(i,j,t-t_d))\Big) \tag{10}$$

where $t_d = 1/fps$, and fps denotes frames per second. m and n denote the width and height of input sampled images. The other notations conform to Eq. (1) that are not restated here.

In the on-line tests, we set up a small arena for the *Colias* robot as shown in Fig. 8. Specifically, there were two cases of arena tests with either singular robot or two robots simultaneously navigated within the arena. As the avoidance behavior is out of the scope of this research, the robot moved forward by default; once a potential collision was detected, it turned to right or left randomly. Importantly, the investigated and compared models were applied as the only collision sensing modality for the autonomous micro-robot. Each model was tested for 60 minutes in total of real world time, half for singular agent and half for two agents, respectively.

The performance of the proposed DNF model in robot implementation is showcased in Fig. 8. The statistical results of success rate of collision detection in the arena tests are listed in Table 4. Generally speaking, the agent with proposed DNF model performed robustly in collision perception during autonomous navigation in the arena, above **93%** of success rate at both tested scenarios. Especially for two robots running together, the agent equipped with the proposed model outperformed all other state-of-the-art methods. For singular robot tests, the LGMD2 model (Fu et al., 2020a) performed the best, the success rate a little higher than the proposed DNF model. The on-line tests consolidated our achievement that the proposed DNF model features computational efficiency and robustness to stabilize collision detection with regard to robotic applications.

6. Further discussions

This paper presents a looming perception model based on the well-known DNF theory. This model effectively generates collision alerts for looming scenarios while remaining unresponsive to other common motion patterns like translation and receding. The model employs two critical mechanisms: adaptive lateral interaction and dynamic activation threshold.

- The adaptive lateral interaction is temporally regulated by input intensity, which is calculated based on the average luminance change per changed pixel. This mechanism eliminates the model's response to translating, elongation, and grating, as these motion patterns induce relatively more consistent and larger lateral interaction scales.

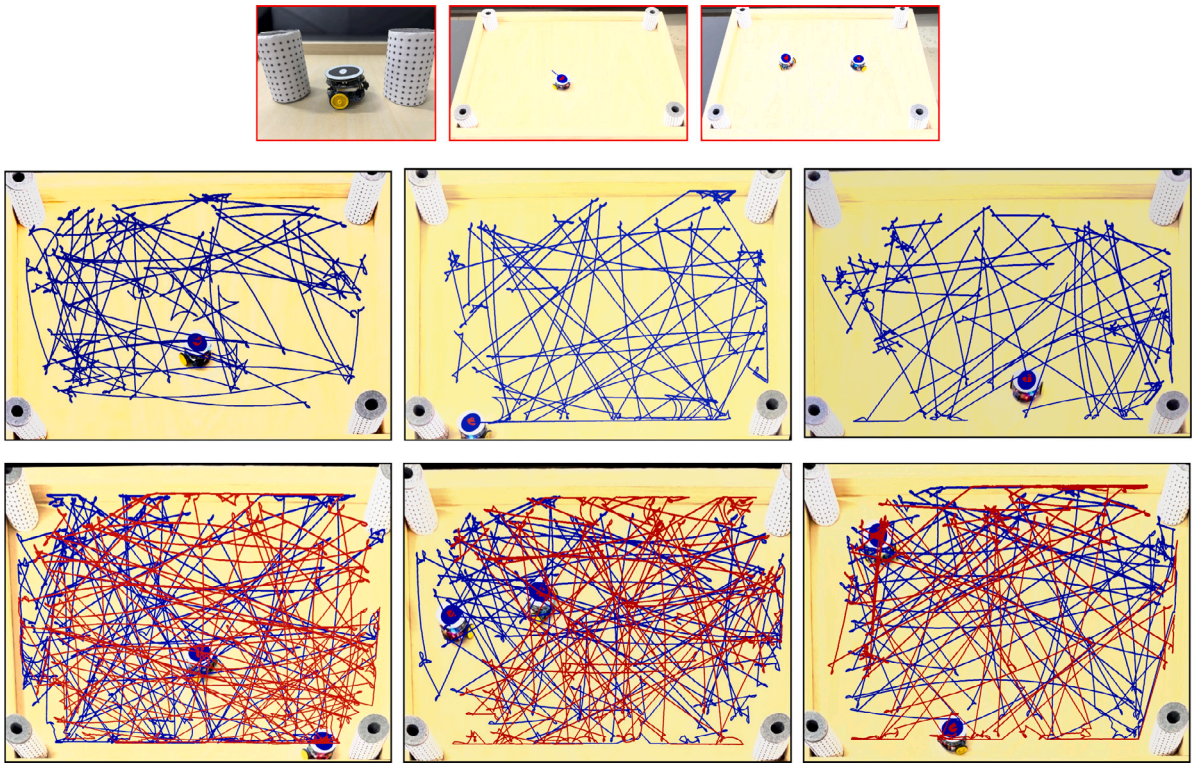

Fig. 8. Robotic implementation of the proposed DNF model for collision perception: top panel represents the arena setting; middle panel illustrates the performance of a single robot navigating within the arena by overtime trajectories (blue lines) generated by a localization algorithm used in a relevant study (Fu et al., 2020a); bottom panel illustrates the performance of two robots running together over time (red and blue lines respectively).

Table 4
Success rate (%) of collision detection in arena tests.

Case	Proposed DNF model	LGMD1	LGMD2	F-LGMD ONn	F-LGMD ONp
1-robot	93.6%	82.9%	**95.5%**	91.4%	87.7%
2-robots	**93.1%**	60.4%	90.0%	77.3%	75.8%

- The dynamic threshold is regulated by previous integrated signals which works effectively to prevent the generation of collision alerts for receding stimuli.

Our ablation study shows the combination of both mechanisms allows the DNF model to accurately detect looming threats while ignoring non-threatening visual movements. The lateral interaction scale is critically important and determined by the variation in σ_1 in the DoG kernel. A larger excitatory lateral interaction scale σ_1 also implies a threefold increase in the inhibitory lateral interaction scale σ_2. Consequently, a larger σ_1 may lead to strong lateral inhibition as the lateral excitation is offset by the inhibition. Conversely, a smaller σ_1 may maintain the lateral interaction within the excitation range, as the summed lateral inhibition is significantly smaller than the lateral excitation. Therefore, the excitatory interaction should be set moderately between 0 and 1 to optimize model performance. As mentioned in Equation (Eq. (3)), σ_1 is regulated by the initial excitatory lateral interaction scale σ_0 and the input intensity. The value of σ_0 is set to 1 for stimuli with a simple background and to 0.618 for more complex testing stimuli. This is because stimuli with a simple background typically yield higher intensity than those with a cluttered background. The input intensity is described as the average luminance change per changed pixel. Although employing the average luminance change across the entire image may yield a more precise representation of input intensity, this approach fails when confronting grating patterns. Grating patterns can be considered as whole-field motion, causing quite high average luminance changes across the image. This results in a significant reduction in the value of σ_1, leading to a strong model response and the generation of a collision alert at the beginning of the stripe's movement. The Appendix also provides insight into how the adaptive lateral interaction affects the convergence of the proposed algorithms. It demonstrates that the larger the initial value of lateral interaction scale is, the more time steps the model requires to converge, which in turn increases the computational time.

The dynamic activation threshold is another key mechanism in this model that shapes looming selectivity. It is inspired by a fundamental neuronal characteristic known as habituation. Specifically, neurons become less responsive if the previous membrane potential consistently increased. This mechanism uses the averaged activation potential of the previous N_{dt} time window outputs. Notably, a similar dynamic threshold mechanism was applied in LGMD-based modeling (Silva et al., 2014). The dynamic threshold is limited to the range of $[0.8, 0.9]$ and updated frame by frame with a step of 0.01. Putting differently, the dynamic threshold in our proposed model functions as part of the spike mechanism and is more likely to reduce the model's response to background noise. This is attributed to the presence of additional cells responsible for distinguishing looming stimuli from receding stimuli. In our proposed model, the dynamic threshold gradually increases for looming stimulus and remain relatively stable for translating-like motion. However, it behaves differently for receding object. Initially, the threshold is set quite high, then gradually decreases, which is effective for suppressing model responses to receding stimuli because the threshold consistently remains higher than the integrated signal, $I_u(t)$, of the model. Typically, a larger value of N_{dt} results in a lower dynamic threshold due to the averaging computation. This can lead to early collision alert generation for looming perception yet incorrect collision

alerts for receding stimuli. Conversely, a lower value of N_{dt} results in a higher dynamic threshold, which can suppress model responses and lead to late or even none collision alerts for looming stimuli.

While the proposed model exhibits remarkable looming selectivity with its relatively simple model structure, the computational demands of solving the DNF equation could restrict its practical applications. It has been shown that implementing a DNF model with propagation delays within the field could potentially reduce the computational time while preserving excellent performance, even in on-line micro-robot tests (Qin et al., 2022a). We have consolidated this point in robot experiments at Section 5.

As demonstrated in Section 5, the proposed method can be integrated into small circuit and sensor implementation for quickly detecting collision danger. This would be extremely useful in application scenarios of industrial robots as the environments are always dynamic and confined by operation range. Calibration techniques flourish on industrial robots and manipulators to improve the interaction within complex environments (Li et al., 2023, 2021). It is also worthy of investigating the incorporation between calibration approaches like Kalman filtering (Li et al., 2022) and our proposed DNF method to enhance the safety of industrial robots.

Furthermore, once the proposed model is shifted to a more comprehensive system for real-world tasks, such as collision-free navigation to a specific goal, optimization algorithms are urgently needed. Evolutionary algorithms have been used to optimize collision detection in LGMD-based models (Fu et al., 2020b; Yue & Rind, 2007, 2013), which may also shed light on improving the performance of the proposed model. Additionally, heuristic search optimization algorithms could be highly beneficial, as these methods have been proven to facilitate path and motion planning in autonomous vehicles (Zlatan Ajanović et al., 2023; Gong, 2022; Reda et al., 2024).

7. Concluding remarks

In this paper, we proposed a novel neural model for looming perception. In addition to the typical formulation of the DNF theory, we incorporated two mechanisms to enhance the looming perception capabilities of our model: the adaptive lateral interaction, which suppresses responses to translating, elongation, and grating stimuli, as well as the dynamic threshold, which restricts responses to receding stimuli. We compared the proposed DNF model with five state-of-the-art, model-based methods in the field of looming perception . Through a series of on-line and off-line experiments, we demonstrated the computational efficiency and robustness of the proposed model. Our model offers a new simplified alternative to the current repository, and successfully extends the DNF theory to looming perception highlighting the effectiveness of instant feedback. Furthermore, this work underscores the great potential of single-field DNF for motion perception tasks.

Despite contributions mentioned above, it is imperative to consider denoising methods to enhance the performance of the proposed model. Moreover, improvements are indispensable to equip the model with the capability to effectively address looming perception in complex and dynamic environments with low contrast.

CRediT authorship contribution statement

Ziyan Qin: Writing – original draft, Visualization, Validation, Software, Methodology, Investigation, Formal analysis, Data curation, Conceptualization. **Qinbing Fu:** Writing – review & editing, Writing – original draft, Supervision, Project administration, Investigation. **Jigen Peng:** Supervision, Funding acquisition, Conceptualization.

Declaration of competing interest

The authors declare that they have no known competing financial interests or personal relationships that could have appeared to influence the work reported in this paper.

Data availability

Data will be made available on request.

Acknowledgments

This research has been funded by the National Natural Science Foundation of China under the Grant No. 12031003, No. 12211540710, No. 62376063, the Social Science Fund of the Ministry of Education of China under the Grant No. 22YJCZH032, and the Innovation Research Grant for the Postgraduates of Guangzhou University. We thank Mr. Hao Chen from Guangzhou University for providing the original proof and conducting a preliminary calibration of the mathematical analysis.

Appendix A. Mathematical analysis

In the Appendix, we provide a mathematical analysis of the convergence of the proposed model with varying adaptive lateral interactions. As stated in the paper, the proposed model accomplishes accurate looming perception through a readily constructed neural field model with adaptive lateral interaction scales and a dynamic threshold-involved spike mechanism. The proposed model receives the input stimuli frame by frame and solves the solution of the differential equation for each position x, y. And these solved solution is served as the membrane potential of the neurons in the receptive field, corresponding one-to-one with the pixel input video. The firing rate of each neuron within the field is then integrated into one temporal signal, generating dynamic thresholds and alerts.

By using the Banach fixed point theorem (Banach, 1922), we mathematically prove that the neural field model has only one stationary solution when considering only the time variation. This serves as a prerequisite for utilizing fixed-point iteration methods in solving the stationary solution of the proposed model. We then analyze the relationship between the iteration times and the varied lateral interaction scales.

To avoid confusion between the evolution time t_i of the differential equation solution and the frames t_f in input video, the proposed model could be rewritten as follows:

$$\frac{\partial u(x,y,t_i,t_f)}{\partial t_i} = -\frac{1}{\tau}u(x,y,t_i,t_f) + S(x,y,t_f) - h + \vartheta\Big(\iint_{\Omega} w(x-i,y-j,t_f)(u(i,j,t_i,t_f))\,dx\,dy\Big) \tag{11}$$

where $t_f > 0$. We compute the activation behavior of the proposed model frame by frame, thus, for a fix frame t_f, the input stimulus and the lateral interaction kernel are fixed as $S(x,y,t_f)$ and $w(x-i,y-j,t_f)$ during the evolution time of the differential equation solution, the proposed model could be rewrite as:

$$\frac{\partial u(x,y,t_i)}{\partial t_i} = -\frac{1}{\tau}u(x,y,t_i) + S(x,y,t_f) - h + \vartheta\Big(\iint_{\Omega} w(x-i,y-j,t_f)(u(i,j,t_i))\,dx\,dy\Big) \tag{12}$$

The threshold of lateral interaction is represented by the sigmoid-like function:

$$\vartheta(u) = \frac{2}{1+e^{-u}} - 1.$$

Now considering a projection $T : \mathcal{L}^p(\Omega\times[0,+\infty)) \to \mathcal{L}^p(\Omega\times[0,+\infty))$ and

$$Tu = \tau S(x,y) - \tau h + \tau\vartheta\Big(\iint_{\Omega} w(x-i,y-j,t_f)(u(i,j,t_i))\,dx\,dy\Big), \tag{13}$$

after ignoring the constant part, we have

$$\|Tu - Tv\|_{\mathcal{L}^p} \tag{14}$$

Table 5
Table of abbreviations.

Abbreviation	Full name
DNF	Dynamic Neural Field
LGMD	Lobula giant movement detector
DoG	Difference of Gaussian
TD	Time Delay
LPTC	Lobula Plate Tangential Cell
UAV	Unmanned Aerial Vehicle
MAV	Micro Aerial Vehicle
LPLC2	Lobula Plate/ Lobula Column Type — II
LGMD1	Computational model proposed by Fu et al. (2018)
LGMD2	Computational model proposed by Fu et al. (2020a)
LGMD1 2022ver .	Computational model proposed by Lei et al. (2022)
F-LGMD ONp	Computational model (with positive feedback on ON contrast) proposed by Chang et al. (2023)
F-LGMD ONn	Computational model (with negative feedback on ON contrast) proposed by Chang et al. (2023)
ODE	Ordinary Differential Equation
DT	Dynamic Threshold
IS	Model Response (Integrated Signal) of the proposed model
tf	Temporal frequency
sf	Spatial frequency
PM	Model Response (Spike) of the proposed model
DNF_{none}	Original DNF model without adaptive lateral interaction and dynamic threshold
DNF_{ai}	Original DNF model with adaptive lateral interaction
DNF_{dt}	Original DNF model with dynamic threshold
TP	True Positive
FP	False Positive
TN	True Negative
FN	False Negative

$$= \tau||\vartheta\Big(\iint_{\Omega} w(x-i,y-j,t_f)(u(i,j,t_i))dx\,dy\Big) - \vartheta\Big(\iint_{\Omega} w(x-i,y-j,t_f)(v(i,j,t_i))\,dx\,dy\Big)||_{\mathcal{L}^p}.$$

Additionally, it can be easily deduced that

$$\begin{aligned}\vartheta(u)-\vartheta(v) &= \frac{2}{1+e^{-u}} - \frac{2}{1+e^{-v}} \\ &= \frac{2e^{-v}-2e^{-x}}{(1+e^{-u})(1+e^{-v})} \\ &\le 2(1-e^{v-u})e^{-v} \\ &\le 2(1-e^{v-u})\end{aligned} \tag{15}$$

Assuming that for any $u, v \in \mathcal{L}^p(\Omega\times[0,+\infty))$, there exists a constant m such that

$$\|\vartheta(u)-\vartheta(v)\|_{\mathcal{L}^p} \le m\|u-v\|_{\mathcal{L}^p},$$

by using the continuity of the exponential function.

Then, by combining Eq. (14) with Young's inequalities (Mitrinovic et al., 2013), we can deduce the following inequalities.

$$\begin{aligned}&\|Tu-Tv\|_{\mathcal{L}^p} \\ &\le \tau m\|\iint_{\Omega} w(x',y',t_f)(u(i,j,t_i)-v(i,j,t_i))\,dx\,dy\|_{\mathcal{L}^p} \\ &\le \tau m\|u-v\|_{\mathcal{L}^p}\cdot\|w\|_{\mathcal{L}^1},\end{aligned} \tag{16}$$

where $x' = x-i, y' = y-j$. Thus, if we let $\tau m\cdot\|w\|_{\mathcal{L}^1} < 1$, there exists a unique $u^* \in \mathcal{B}$ satisfying the equation $Tu^* = u^*$ according to Banach fixed point theorem (Banach, 1922). Consequently, the neural field model (1) possesses a unique stationary solution.

We then proceed to construct the fixed point iteration algorithm as follows: $u_n = T^n u_0$. We set the initial value as $u_0 = -h = -0.2$, and the iteration terminates when $u_n - u_{n-1} \le 0.001$ or $n \ge 10$.

We next discuss how the number of iterations required to solve the stationary solution varies with the adaptive lateral interaction scales.

The lateral interaction kernel is given as the DoG kernel with a "Mexican hat" shape, and

$$\begin{aligned}\|w\|_{\mathcal{L}^1} &= \int_0^{\infty}\iint_{\mathbf{R}^2}\frac{3}{2}\exp\Big(-\frac{(x^2+y^2)}{2\sigma_1(t)^2}\Big) \\ &\quad -\frac{1}{2}\exp\Big(-\frac{(x^2+y^2)}{2\sigma_{u,2}(t)^2}\Big)dxdydt \\ &= \int_0^{\infty}\iint_{\mathbf{R}^2}\frac{3}{2}\exp\Big(-\frac{1}{2}\frac{x^2}{\sigma_1(t)^2}-\frac{1}{2}\frac{y^2}{\sigma_1(t)^2}\Big) \\ &\quad -\frac{1}{2}\exp\Big(-\frac{1}{2}\frac{x^2}{\sigma_2(t)^2}-\frac{1}{2}\frac{y^2}{\sigma_2(t)^2}\Big)dxdydt\end{aligned} \tag{17}$$

Where $t \ge 0$ is for the general analysis of lateral interaction kernel. Since $\sigma_2(t) = 3\sigma_1(t)$, and let $x' = \frac{x}{\sigma_2(t)}, y' = \frac{y}{\sigma_2(t)}$ the above equality could be rewritten as an inequality according to Minkowski's inequality (Mulholland, 1949):

$$\begin{aligned}\|w\|_{\mathcal{L}^1} &= \int_0^{\infty}\iint_{\mathbf{R}^2}\frac{3}{2}\exp\Big(-\frac{1}{2}\Big(\frac{9x^2}{\sigma_2(t)^2}+\frac{9x^2}{\sigma_2(t)^2}\Big)\Big) \\ &\quad -\frac{1}{2}\exp\Big(-\frac{1}{2}\Big(\frac{x^2}{\sigma_2(t)^2}+\frac{y^2}{\sigma_2(t)^2}\Big)\Big)dxdydt \\ &= \int_0^{\infty}\iint_{\mathbf{R}^2}\frac{3}{2}\exp\Big(-\frac{3}{2}(x'^2+y'^2)\Big) \\ &\quad -\frac{1}{2}\exp\Big(-\frac{1}{2}(x'^2+y'^2)\Big)dx\sigma_2(t)dy\sigma_2(t)dt \\ &= \int_0^{\infty}\sigma_2^2(t)\iint_{\mathbf{R}^2}\frac{3}{2}\exp\Big(-\frac{3}{2}(x^2+y^2)\Big) \\ &\quad -\frac{1}{2}\exp\Big(-\frac{1}{2}(x^2+y^2)\Big)dxdydt \\ &\le \int_0^{\infty}\sigma_2^2(t)\Big(\frac{3}{2}\cdot\frac{2}{3}\pi+\frac{1}{2}\cdot 2\pi\Big)dt \\ &= 2\pi\int_0^{\infty}\sigma_2^2(t)dt = 18\pi\int_0^{\infty}\sigma_1^2(t)dt\end{aligned} \tag{18}$$

Now we back to consider the relationship between the iteration times and the varied lateral interaction scales. Under the same assumption as previous, for any $u, v \in \mathcal{B}\subset\mathcal{L}^p(\Omega\times[0,+\infty))$, there exists a constant m, for any$p \ge 1$, we have

$$\|Tu-Tv\|_{\mathcal{L}^p} \le 18\tau m\pi\sigma_1^2(t_f)\cdot\|u-v\|_{\mathcal{L}^p}. \tag{19}$$

According to fix point iteration algorithms we construct above, we have

$$\begin{aligned}&\|u_n-u_{n-1}\|_{\mathcal{L}^p} \\ &= \|Tu_{n-1}-Tu_{n-2}\|_{\mathcal{L}^p} \\ &\le 18\tau m\pi\sigma_1^2(t_f)\cdot\|u_{n-1}-u_{n-2}\|_{\mathcal{L}^p} \\ &\le (18\tau m\pi)^{n-1}\cdot(\sigma_1^2(t_f))^{n-1}\cdot\|Tu_0-u_0\|_{\mathcal{L}^p}.\end{aligned} \tag{20}$$

Table 6
Table of variables.

Variables	Definition	Value or source
$m \times n$	The resolution of input video; The number of neurons within the DNF.	Adapted from input.
$u(x, y, t)$	The membrane potential of a neuron which receives input from the pixel that located at spatial coordinates (x, y) at time t.	Obtained through Eq. (1).
$L(x, y, t)$	The gray-scale brightness of the pixel that located at spatial coordinates (x, y) at time t.	Adapted from input.
τ	Time scale of the neural activation within the DNF .	1, same as (Jin et al., 2021).
$S(x, y, t)$	External input for $u(x, y, t)$.	Adapted from $L(x, y, t)$ and $L(x, y, t-1)$.
$\vartheta(\cdot)$	Threshold function for lateral interaction	Sigmoid-like function.
h	Resting level of the neurons with DNF	0.2, same as (Jin et al., 2021).
$w(x, y, t)$	Lateral interaction kernel with Mexican-hat shape.	DoG Kernel; Obtained through Eq. (3).
σ_0	Initial excitatory lateral interaction scale	1 for stimuli with simple background; 0.618 for stimuli with cluttered background.
$\sigma_1(t)$	Excitatory lateral interaction scale	Obtained through Eq. (4).
$\sigma_2(t)$	Inhibitory lateral interaction scale	Adapted from $\sigma_1(t)$, $\sigma_2(t) = 3\sigma_1(t)$.
$\theta(\cdot)$	Activation function of neurons.	Normalized *tanh* function, source from (Dayan & Abbott, 2002).
$I_u(t)$	Integrated signal of DNF.	Obtained through Eq. (5).
$I_{thre}(t)$	Dynamic threshold.	Obtained through Eq. (6).
N_{dt}	Time Window for dynamic threshold.	5.
N_{spk}	The number of spike within a specific time that are required to trigger an alert.	4, same as (Fu et al., 2018).

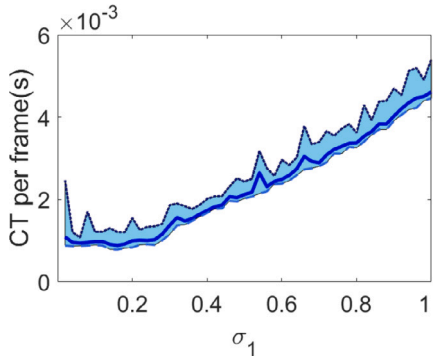

Fig. 9. During the processing of dark square approaching scenarios, the computational time per frame (abbreviated as CT in the figure) exhibits variation with respect to σ_1 in lateral interaction. Specifically, as the value of σ_1 increases, the computational time per frame also experiences corresponding growth.

As the value of $\sigma_1(t_f)$ increases, the difference between u_n and u_{n-1} also increases, leading to a higher number of iterations. Consequently, the computational time will also rise accordingly (Fig. 9).

As the value of σ_1 is gradually decreased during looming process, gradually increase during receding and relatively stable for translating-like motion, it can be deduced that the iteration times will progressively decrease in response to looming stimuli, increase for receding stimuli, and remain relatively stable for translating and grating stimuli (Fig. 10).

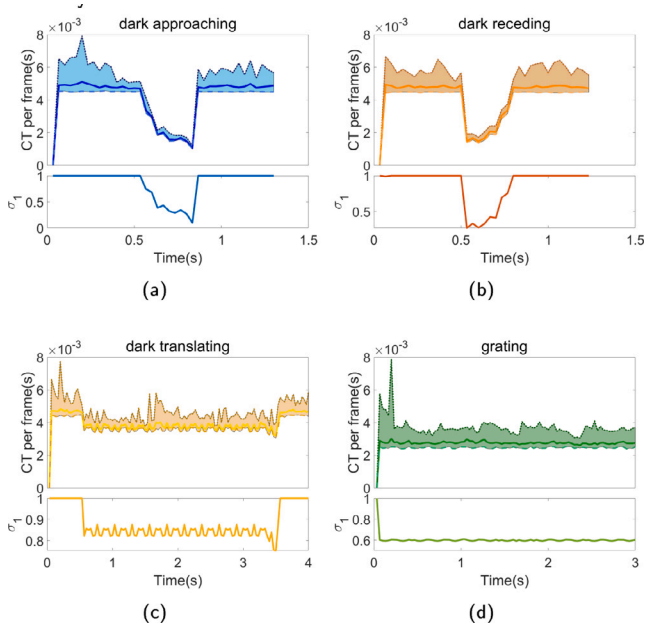

Fig. 10. The computational time (abbreviated as CT in the figure) per frame when the proposed model processing the four basic synthetic stimuli: (a) dark square approaching, (b) dark square receding, (c) dark bar translating, (d) grating. The shades in each sub-figure represent the variance of computational time per frame for 10 runs, while the solid line represents the average computational time per frame in these 10 runs.

Appendix B. Table of abbreviations

See Table 5.

Appendix C. Table of variables

See Table 6.

Appendix D. Supplementary data

Supplementary material related to this article can be found online at https://doi.org/10.1016/j.neunet.2024.106502.

References

Ajanović, Z., Regolin, E., Shyrokau, B., Ćatić, H., Horn, M., & Ferrara, A. (2023). Search-based task and motion planning for hybrid systems: Agile autonomous vehicles. *Engineering Applications of Artificial Intelligence*, *121*, Article 105893. http://dx.doi.org/10.1016/j.engappai.2023.105893, URL https://www.sciencedirect.com/science/article/pii/S0952197623000775.

Amari, S. (1977). Dynamics of pattern formation in lateral-inhibition type neural fields. *Biological Cybernetics*, *27*, 77–87. http://dx.doi.org/10.1007/BF00337259.

Banach, S. (1922). Sur les opérations dans les ensembles abstraits et leur application aux équations intégrales. *Fundamenta mathematicae*, *3*(1), 133–181. http://dx.doi.

org/10.4064/fm-3-1-133-181.
Borst, A. (2014). Fly visual course control: behaviour, algorithms and circuits. *Nature Reviews Neuroscience*, *15*(9), 590–599. http://dx.doi.org/10.1038/nrn3799.
Brandt, R. D., & Lin, F. (1999). Adaptive interaction and its application to neural networks. *Information Sciences*, *121*(3), 201–215. http://dx.doi.org/10.1016/S0020-0255(99)00090-0.
Burlakov, E., Zhukovskiy, E., & Verkhlyutov, V. (2021). Neural field equations with neuron-dependent heaviside-type activation function and spatial-dependent delay. *Mathematical Methods in the Applied Sciences*, *44*(15), 11895–11903. http://dx.doi.org/10.1002/mma.6661.
Chang, Z., Fu, Q., Chen, H., Li, H., & Peng, J. (2023). A look into feedback neural computation upon collision selectivity. *Neural Networks*, *166*, 22–37. http://dx.doi.org/10.1016/j.neunet.2023.06.039.
Cigla, C., Brockers, R., & Matthies, L. (2017). Image-based visual perception and representation for collision avoidance. In *2017 IEEE conference on computer vision and pattern recognition workshops* (pp. 421–429). http://dx.doi.org/10.1109/CVPRW.2017.57.
Dayan, P., & Abbott, L. F. (2002). Theoretical neuroscience: Computational and mathematical modeling of neural systems. MIT Press, https://mitpress.mit.edu/9780262041997/theoretical-neuroscience/.
Ding, J., Dong, B., Heide, F., Ding, Y., Zhou, Y., Yin, B., & Yang, X. (2022). Biologically inspired dynamic thresholds for spiking neural networks. In S. Koyejo, S. Mohamed, A. Agarwal, D. Belgrave, K. Cho, & A. Oh (Eds.), *35*, *Advances in neural information processing systems* (pp. 6090–6103). Curran Associates, Inc., http://dx.doi.org/10.48550/arXiv.2206.04426.
Erlhagen, W., & Schöner, G. (2002). Dynamic field theory of movement preparation. *Psychological Review*, *109*(3), 545–572. http://dx.doi.org/10.1037/0033-295x.109.3.545.
Fotowat, H., & Gabbiani, F. (2011). Collision detection as a model for sensory-motor integration. *Annual Review of Neuroscience*, *34*(1), 1–19. http://dx.doi.org/10.1146/annurev-neuro-061010-113632.
Franceschini, N. (2014). Small brains, smart machines: From fly vision to robot vision and back again. *Proceedings of the IEEE*, *102*(5), 751–781. http://dx.doi.org/10.1109/JPROC.2014.2312916.
Fu, Q., Hu, C., Peng, J., Rind, F. C., & Yue, S. (2020). A robust collision perception visual neural network with specific selectivity to darker objects. *IEEE Transactions on Cybernetics*, *50*(12), 5074–5088. http://dx.doi.org/10.1109/TCYB.2019.2946090.
Fu, Q., Hu, C., Peng, J., & Yue, S. (2018). Shaping the collision selectivity in a looming sensitive neuron model with parallel ON and OFF pathways and spike frequency adaptation. *Neural Networks*, *106*, 127–143. http://dx.doi.org/10.1016/j.neunet.2018.04.001.
Fu, Q., Wang, H., Hu, C., & Yue, S. (2019). Towards computational models and applications of insect visual systems for motion perception: A review. *Artificial Life 25*, *25*(3), 263–311. http://dx.doi.org/10.1162/artl_a_00297.
Fu, Q., Wang, H., Peng, J., & Yue, S. (2020). Improved collision perception neuronal system model with adaptive inhibition mechanism and evolutionary learning. *IEEE Access*, *8*, 108896–108912. http://dx.doi.org/10.1109/ACCESS.2020.3001396.
Gabbiani, F., Krapp, H. G., Koch, C., & Laurent, G. (2002). Multiplicative computation in a visual neuron sensitive to looming. *Nature*, *420*(6913), 320–324. http://dx.doi.org/10.1038/nature01190.
Gabbiani, F., Krapp, H. G., & Laurent, G. (1999). Computation of object approach by a wide-field, motion-sensitive neuron. *Journal of Neuroscience*, *19*(3), 1122–1141. http://dx.doi.org/10.1523/JNEUROSCI.19-03-01122.1999.
Gabbiani, F., Mo, C., & Laurent, G. (2001). Invariance of angular threshold computation in a wide-field looming-sensitive neuron. *Journal of Neuroscience*, *21*(1), 314–329. http://dx.doi.org/10.1523/JNEUROSCI.21-01-00314.2001.
Giese, M. A. (1999). Dynamic neural field theory for motion perception. New York: Springer Science+Business Media, http://dx.doi.org/10.1007/978-1-4615-5581-0.
Gong, F. (2022). [Retracted] application of artificial intelligence computer intelligent heuristic search algorithm. *Advances in Multimedia*, *2022*(1), Article 5178515. http://dx.doi.org/10.1155/2022/5178515, URL https://onlinelibrary.wiley.com/doi/abs/10.1155/2022/5178515.
Gouda, W., Gomaa, W., & Ogawa, T. (2013). Vision based SLAM for humanoid robots: A survey. In *2013 second international Japan-Egypt conference on electronics, communications and computers (JEC-eCC)* (pp. 170–175). http://dx.doi.org/10.1109/JEC-ECC.2013.6766407.
Green, W. E., & Oh, P. Y. (2008). Optic-flow-based collision avoidance. *IEEE Robotics & Automation Magazine*, *15*(1), 96–103. http://dx.doi.org/10.1109/MRA.2008.919023.
Hatsopoulos, N., Gabbiani, F., & Laurent, G. (1995). Elementary computation of object approach by a wide-field visual neuron. *Science*, *270*(5238), 1000–1003. http://dx.doi.org/10.1126/science.270.5238.1000.
Heiberg, A., Larsen, T. N., Meyer, E., Rasheed, A., San, O., & Varagnolo, D. (2022). Risk-based implementation of COLREGs for autonomous surface vehicles using deep reinforcement learning. *Neural Networks*, *152*, 17–33. http://dx.doi.org/10.1016/j.neunet.2022.04.008.
Hu, Z., Yang, L., Du, Z., Na, Y., & Su, Y. (2022). An edge detection algorithm for neutrosophic set based on adaptive threshold. Research Square, http://dx.doi.org/10.21203/rs.3.rs-1860703/v1.
Hua, M., Luan, H., Peng, J., Yue, S., & Fu, Q. (2022). Shaping the ultra-selectivity of a looming detection neural network from non-linear correlation of radial motion. In *The 2022 international joint conference on neural networks* (pp. 1–8). http://dx.doi.org/10.1109/IJCNN55064.2022.9892408.
Jin, D., Qin, Z., Yang, M., & Chen, P. (2021). A novel neural model with lateral interaction for learning tasks. *Neural Computation*, *33*(2), 528–551. http://dx.doi.org/10.1162/neco_a_01345.
Jones, P. W., & Gabbiani, F. (2012). Logarithmic compression of sensory signals within the dendritic tree of a collision-sensitive neuron. *Journal of Neuroscience*, *32*(14), 4923–4934. http://dx.doi.org/10.1523/JNEUROSCI.5777-11.2012.
Kamkar, S., Moghaddam, H. A., Lashgari, R., & Erlhagen, W. (2022). Brain-inspired multiple-target tracking using dynamic neural fields. *Neural Networks*, *151*, 121–131. http://dx.doi.org/10.1016/j.neunet.2022.03.026.
Klapoetke, N. C., Nern, A., Peek, M. Y., Rogers, E. M., Breads, P., Rubin, G. M., Reiser, M. B., & Card, G. M. (2017). Ultra-selective looming detection from radial motion opponency. *Nature*, *551*(7679), 237–241. http://dx.doi.org/10.1038/nature24626.
Kwessi, E. (2021). Discrete dynamics of dynamic neural fields. *Frontiers in Computational Neuroscience*, *15*, Article 699658. http://dx.doi.org/10.3389/fncom.2021.699658.
Lei, F., Peng, Z., Liu, M., Peng, J., Cutsuridis, V., & Yue, S. (2022). A robust visual system for looming cue detection against translating motion. *IEEE Transactions on Neural Networks and Learning Systems*, *34*(11), 8362–8376. http://dx.doi.org/10.1109/TNNLS.2022.3149832.
Levina, A., Herrmann, J. M., & Geisel, T. (2009). Phase transitions towards criticality in a neural system with adaptive interactions. *Physical Review Letters*, *102*, Article 118110. http://dx.doi.org/10.1103/PhysRevLett.102.118110.
Li, Z., Li, S., Bamasag, O. O., Alhothali, A., & Luo, X. (2023). Diversified regularization enhanced training for effective manipulator calibration. *IEEE Transactions on Neural Networks and Learning Systems*, *34*(11), 8778–8790. http://dx.doi.org/10.1109/TNNLS.2022.3153039.
Li, Z., Li, S., Francis, A., & Luo, X. (2022). A novel calibration system for robot arm via an open dataset and a learning perspective. *IEEE Transactions on Circuits and Systems II: Express Briefs*, *69*(12), 5169–5173. http://dx.doi.org/10.1109/TCSII.2022.3199158.
Li, Z., Li, S., & Luo, X. (2021). An overview of calibration technology of industrial robots. *IEEE/CAA Journal of Automatica Sinica*, *8*(1), 23–36. http://dx.doi.org/10.1109/JAS.2020.1003381.
Liu, D., Bellotto, N., & Yue, S. (2020). Deep spiking neural network for video-based disguise face recognition based on dynamic facial movements. *IEEE Transactions on Neural Networks and Learning Systems*, *31*, 1843–1855. http://dx.doi.org/10.1109/TNNLS.2019.2927274.
Liu, D., & Yue, S. (2017). Fast unsupervised learning for visual pattern recognition using spike timing dependent plasticity. *Neurocomputing*, *249*, 212–224. http://dx.doi.org/10.1016/j.neucom.2017.04.003.
Macias-Garcia, E., Galeana-Perez, D., & Bayro-Corrochano, E. (2020). CNN based perception system for collision avoidance in mobile robots using stereo vision. In *2020 international joint conference on neural networks* (pp. 1–7). http://dx.doi.org/10.1109/IJCNN48605.2020.9206747.
Mcfadyen, A., & Mejias, L. (2016). A survey of autonomous vision-based see and avoid for unmanned aircraft systems. *Progress in Aerospace Sciences*, *80*, 1–17. http://dx.doi.org/10.1016/j.paerosci.2015.10.002.
McManus, J. N. J., Li, W., & Gilbert, C. D. (2011). Adaptive shape processing in primary visual cortex. *Proceedings of the National Academy of Sciences*, *108*(24), 9739–9746. http://dx.doi.org/10.1073/pnas.1105855108.
Meng, F., & Yang, D. (2020). Research of UAV location control system based on SINS, GPS and optical flow. *1*, In *2020 IEEE international conference on information technology,big data and artificial intelligence* (pp. 495–498). http://dx.doi.org/10.1109/ICIBA50161.2020.9276977.
Milde, M. B., Bertrandn, O. J., Benosmanz, R., Egelhaaf, M., & Chicca, E. (2015). Bioinspired event-driven collision avoidance algorithm based on optic flow. In *2015 international conference on event-based control, communication, and signal processing* (pp. 1–7). http://dx.doi.org/10.1109/EBCCSP.2015.7300673.
Mitrinovic, D. S., Pecaric, J., & Fink, A. M. (2013). Classical and new inequalities in analysis. *vol. 61*, Springer Science & Business Media, http://dx.doi.org/10.1007/978-94-017-1043-5.
Mukhtar, A., Xia, L., & Tang, T. B. (2015). Vehicle detection techniques for collision avoidance systems: A review. *IEEE Transactions on Intelligent Transportation Systems*, *16*(5), 2318–2338. http://dx.doi.org/10.1109/TITS.2015.2409109.
Mulholland, H. (1949). On generalizations of Minkowski's inequality in the form of a triangle inequality. *Proceedings of the London Mathematical Society s2-51*, 294–307. http://dx.doi.org/10.1112/plms/s2-51.4.294.
Olson, E. G. N., Wiens, T. K., & Gray, J. R. (2021). A model of feedforward, global, and lateral inhibition in the locust visual system predicts responses to looming stimuli. *Biological Cybernetics*, *115*(3), 245–265. http://dx.doi.org/10.1007/s00422-021-00876-8.
O'shea, M., Rowell, C. H. F., & Williams, J. L. D. (1974). The anatomy of a locust visual interneurone: the descending contralateral movement detector. *Journal of Experimental Biology*, *60*, 1–12. http://dx.doi.org/10.1242/jeb.60.1.1.

Park, S., Lee, K., Song, H., Cho, J., Park, S.-Y., & Yoon, E. (2019). Low-power, bio-inspired time-stamp-based 2-D optic flow sensor for artificial compound eyes of micro air vehicles. *IEEE Sensors Journal*, *19*(24), 12059–12068. http://dx.doi.org/10.1109/JSEN.2019.2938559.

Pentland, A. P. (1987). A new sense for depth of field. *IEEE Transactions on Pattern Analysis and Machine Intelligence*, *PAMI-9*(4), 523–531. http://dx.doi.org/10.1109/TPAMI.1987.4767940.

Qin, Z., Fu, Q., Jin, D., & Peng, J. (2022). A looming perception model based on dynamic neural field. *Available at SSRN 4248213*.

Qin, Z., Peng, J., & Jin, D. (2022). A method for support neuron selection in NMLI. *Neurocomputing*, *489*, 52–58. http://dx.doi.org/10.1016/j.neucom.2022.03.030.

Quinton, J.-C., & Goffart, L. (2018). A unified dynamic neural field model of goal directed eye movements. *Connection Science*, *30*, 20–52. http://dx.doi.org/10.1080/09540091.2017.1351421.

Rafiee, G., Dlay, S., & Woo, W. (2013). Region-of-interest extraction in low depth of field images using ensemble clustering and difference of Gaussian approaches. *Pattern Recognition*, *46*(10), 2685–2699. http://dx.doi.org/10.1016/j.patcog.2013.03.006.

Reda, M., Onsy, A., Haikal, A. Y., & Ghanbari, A. (2024). Path planning algorithms in the autonomous driving system: A comprehensive review. *Robotics and Autonomous Systems*, *174*, Article 104630. http://dx.doi.org/10.1016/j.robot.2024.104630, URL https://www.sciencedirect.com/science/article/pii/S0921889024000137.

Reich, G. M., Antoniou, M. N., & Baker, C. J. (2020). Memory-enhanced cognitive radar for autonomous navigation. *Iet Radar Sonar and Navigation*, *14*, 1287–1296. http://dx.doi.org/10.1049/iet-rsn.2019.0409.

Rind, F. C. (1996). Intracellular characterization of neurons in the locust brain signaling impending collision. *Journal of Neurophysiology*, *75*(3), 986–995. http://dx.doi.org/10.1152/jn.1996.75.3.986.

Rind, F. C., & Bramwell, D. I. (1996). Neural network based on the input organization of an identified neuron signaling impending collision. *Journal of Neurophysiology*, *75*(3), 967–985. http://dx.doi.org/10.1152/jn.1996.75.3.967.

Salt, L., Indiveri, G., & Sandamirskaya, Y. (2017). Obstacle avoidance with LGMD neuron: Towards a neuromorphic uav implementation. In *2017 IEEE international symposium on circuits and systems* (pp. 1–4). http://dx.doi.org/10.1109/ISCAS.2017.8050976.

Schmidt, B., & Wang, L. (2014). Depth camera based collision avoidance via active robot control. *Journal of Manufacturing Systems*, *33*(4), 711–718. http://dx.doi.org/10.1016/j.jmsy.2014.04.004.

Serres, J. R., & Ruffier, F. (2017). Optic flow-based collision-free strategies: From insects to robots. *Arthropod Structure & Development*, *46*(5), 703–717. http://dx.doi.org/10.1016/j.asd.2017.06.003.

Shi, X., Li, Z., & Yu, H. (2021). Adaptive threshold cascade faster RCNN for domain adaptive object detection. *Multimedia Tools and Applications*, *80*(16), 25291–25308. http://dx.doi.org/10.1007/s11042-021-10917-w.

Silva, A. C., Silva, J., & dos Santos, C. P. (2014). A modified LGMD based neural network for automatic collision detection. In *Informatics in control, automation and robotics. lecture notes in electrical engineering* (pp. 217–233). http://dx.doi.org/10.1007/978-3-319-03500-0_14.

Solak, M., Faydasicok, O., & Arik, S. (2023). A general framework for robust stability analysis of neural networks with discrete time delays. *Neural Networks*, *162*, 186–198. http://dx.doi.org/10.1016/j.neunet.2023.02.040.

Spek, L., Kuznetsov, Y. A., & van Gils, S. A. (2020). Neural field models with transmission delays and diffusion. *Journal of Mathematical Neuroscience*, *10*(1), 21. http://dx.doi.org/10.1186/s13408-020-00098-5.

Tan, C. K., Plöger, P. G., & Trappenberg, T. P. (2016). A neural field approach to obstacle avoidance. *9904*, In *2016: advances in artificial intelligence. KI 2016* (pp. 69–87). http://dx.doi.org/10.1007/978-3-319-46073-4.

Wang, H., Dewell, R. B., Zhu, Y., & Gabbiani, F. (2018). Feedforward inhibition conveys time-varying stimulus information in a collision detection circuit. *Current Biology*, *28*(10), 1509–1521 e3. http://dx.doi.org/10.1016/j.cub.2018.04.007.

Woodman, G. F., Vogel, E. K., & Luck, S. J. (2001). Visual search remains efficient when visual working memory is full. *Psychological Science*, *12*(3), 219–224. http://dx.doi.org/10.1111/1467-9280.00339.

Yue, S., & Rind, F. C. (2006). Collision detection in complex dynamic scenes using an LGMD-based visual neural network with feature enhancement. *IEEE Transactions on Neural Networks*, *17*(3), 705–716. http://dx.doi.org/10.1109/TNN.2006.873286.

Yue, S., & Rind, F. C. (2007). A synthetic vision system using directionally selective motion detectors to recognize collision. *Artificial Life 25*, *13*(2), 93–122. http://dx.doi.org/10.1162/artl.2007.13.2.93.

Yue, S., & Rind, F. C. (2013). Redundant neural vision systems—Competing for collision recognition roles. *IEEE Transactions on Autonomous Mental Development*, *5*(2), 173–186. http://dx.doi.org/10.1109/TAMD.2013.2255050.

Yue, S., Rind, F. C., Keil, M. S., Cuadri, J., & Stafford, R. (2006). A bio-inspired visual collision detection mechanism for cars: Optimisation of a model of a locust neuron to a novel environment. *Neurocomputing*, *69*(13), 1591–1598. http://dx.doi.org/10.1016/j.neucom.2005.06.017.

Zhao, J., Ma, X., Fu, Q., Hu, C., & Yue, S. (2019). An LGMD based competitive collision avoidance strategy for UAV. In *Artificial intelligence applications and innovations* (pp. 80–91). Springer International Publishing.

Zhao, J., Wang, H., Bellotto, N., Hu, C., Peng, J., & Yue, S. (2023). Enhancing lgmd's looming selectivity for UAV with spatial-temporal distributed presynaptic connections. *IEEE Transactions on Neural Networks and Learning Systems*, *34*, 2539–2553. http://dx.doi.org/10.1109/TNNLS.2021.3106946.

Zhao, J., Xi, S., Li, Y., Guo, A., & Wu, Z. (2023). A fly inspired solution to looming detection for collision avoidance. *iScience*, *26*(4), Article 106337. http://dx.doi.org/10.1016/j.isci.2023.106337.

Zhao, T., Yao, J., Gong, C., & Wang, Y. (2022). Wireless ultraviolet light MIMO assisted UAV direction perception and collision avoidance method. *Physical Communication*, *54*, Article 101815. http://dx.doi.org/10.1016/j.phycom.2022.101815.

Zhou, B., Li, Z., Kim, S., Lafferty, J., & Clark, D. A. (2022). Shallow neural networks trained to detect collisions recover features of visual loom-selective neurons. *eLife*, *11*, Article e72067. http://dx.doi.org/10.7554/eLife.72067.

Zhou, X., Molina, R., Ma, Y., Wang, T., & Ni, D. (2020). Parameter-free Gaussian PSF model for extended depth of field in brightfield microscopy. *IEEE Transactions on Image Processing*, *29*, 3227–3238. http://dx.doi.org/10.1109/TIP.2019.2957941.

Zhu, Y., Dewell, R. B., Wang, H., & Gabbiani, F. (2018). Pre-synaptic muscarinic excitation enhances the discrimination of looming stimuli in a collision-detection neuron. *Cell Reports*, *23*(8), 2365–2378. http://dx.doi.org/10.1016/j.celrep.2018.04.079.